Angle-of-Attack Convergence and Windward-Meridian Rotation Rate of Rolling Reentry Vehicles

Prepared by DANIEL H. PLATUS
Aerodynamics and Propulsion Research Laboratory

69 JAN 98

Laboratory Operations
AEROSPACE CORPORATION

Prepared for SPACE AND MISSILE SYSTEMS ORGANIZATION
AIR FORCE SYSTEMS COMMAND
LOS ANGELES AIR FORCE STATION
Los Angeles, California

THIS DOCUMENT HAS BEEN APPROVED FOR PUBLIC
RELEASE AND SALE: ITS DISTRIBUTION IS UNLIMITED

ANGLE-OF-ATTACK CONVERGENCE AND
WINDWARD-MERIDIAN ROTATION RATE
OF ROLLING REENTRY VEHICLES

Prepared by

Daniel H. Platus
Aerodynamics and Propulsion Research Laboratory

69 JAN 08

Prepared for

FOREWORD

Approved

Walter R. Warren, Jr., Director
Aerodynamics and Propulsion Research
  Laboratory

Edward M. Williams, Jr.
2nd Lieutenant, United States Air Force
Project Officer

BLANK PAGES
IN THIS
DOCUMENT
WERE NOT
FILMED

ABSTRACT

A simple expression is derived for the influence of roll acceleration on the angle-of-attack convergence of rolling reentry vehicles with pitch or yaw damping. Also included is an analysis of the windward-meridian rotation rate of the rolling vehicle, which is coupled through the gyroscopic equations of motion to the angle of attack and roll rate. It is found that two modes of motion exist for which the windward meridian is generally oscillatory in one mode and rotary in the other (i.e., the vehicle either oscillates about its roll axis relative to the wind or rotates continuously in one direction). The mode of motion depends on the initial reentry conditions, and it is shown that a roll-induced instability can occur whereby the motion changes from the oscillatory mode to the more stable rotary mode. The analytical approximations are compared with computer solutions of the complete equations of motion.

CONTENTS

FIGURES

1. INTRODUCTION

Of particular interest in the performance evaluation of a reentry vehicle is its angle-of-attack behavior during reentry through the atmosphere. Understanding of the angle-of-attack behavior is essential for prediction of the vehicle's trajectory and for assessment of the thermal requirements of the vehicle's heat-protective system. In addition to the heating prediction, a knowledge of the windward-meridian rotation rate is required if one is to couple the heating or ablation rate prediction with the vehicle dynamic motion.

This paper treats the influence of roll rate and roll acceleration on the angle-of-attack convergence of rolling reentry vehicles and presents a technique for predicting the windward-meridian rotation rate, which is coupled through the gyroscopic equations of motion to the angle of attack and roll rate. The windward-meridian rotation rate is also dependent on the initial (exoatmospheric) motion, and it is found that two modes of motion exist for which the windward-meridian is generally oscillatory in one mode and rotary in the other (i.e., the vehicle either oscillates about its roll axis relative to the wind or rotates continuously in one direction). It is further shown that the rotary mode is more stable, although either mode can persist, depending on the initial conditions, and an instability can occur with the presence of roll acceleration whereby the motion changes from the oscillatory mode to the more stable rotary mode. A criterion is presented for predicting this instability, which occurs only when the roll rate is large relative to the natural pitch frequency of the vehicle.

The angle-of-attack convergence behavior of rolling reentry vehicles has been studied, and a number of papers on the subject are reported in the literature.[1-5] All of these, however, treat the case of constant roll rate; only one includes the effect of pitch or yaw damping on the convergence envelope,[1] and none discusses in any detail the influence of exoatmospheric conditions on the subsequent angle-of-attack convergence and vehicle motion. Because of the susceptibility of high-performance reentry vehicles to roll

-1-

resonance and other phenomena that can cause significant roll rate excursions, it is of interest to assess the influence of roll acceleration on the angle-of-attack convergence and on the windward-meridian rotation behavior.

The present study treats the vehicle motion during the period in which, because of misalignment with the flight path during reentry, the angle of attack is large relative to the trim angle of attack from mass or configurational asymmetries. The quasi-steady or mean value of the angle-of-attack oscillation envelope is obtained as a function of time (or altitude) during this period.

II. EQUATIONS OF MOTION

The vehicle motion is described in terms of the Euler angles Ψ, ϕ, θ, as shown in Fig. 1. If the principal moments of inertia about the ξ, η, ζ axes are I, I, I_x, respectively (pitch, yaw, roll), and the aerodynamic moments about these axes are M_ξ, M_η, M_ζ, the moment equations of motion in terms of the Euler angles may be written[6]

$$M_\xi = I\ddot{\theta} + I_x p\dot{\Psi} \sin\theta - I\dot{\Psi}^2 \sin\theta \cos\theta$$

$$M_\eta = I \frac{d}{dt}(\dot{\Psi} \sin\theta) + I\dot{\theta}\dot{\Psi} \cos\theta - I_x p\dot{\theta} \qquad (1)$$

$$M_\zeta = I_x \frac{dp}{dt}$$

where the roll rate p is defined by

$$p = \dot{\phi} + \dot{\Psi} \cos\theta. \qquad (2)$$

The angular rate $\dot{\phi}$ is the windward-meridian rotation rate, i.e., the roll rate with respect to the wind. It is assumed that the aerodynamic moments consist only of pitch or yaw moments from angle of attack, an arbitrary roll moment, and pitch and yaw damping moments. It is further assumed that the vehicle is aerodynamically axisymmetric (i.e., $C_{N_\alpha} = C_{N_\beta}$), so that the restoring torque from angle of attack is independent of the roll orientation ϕ and dependent only on θ. The moments are then written
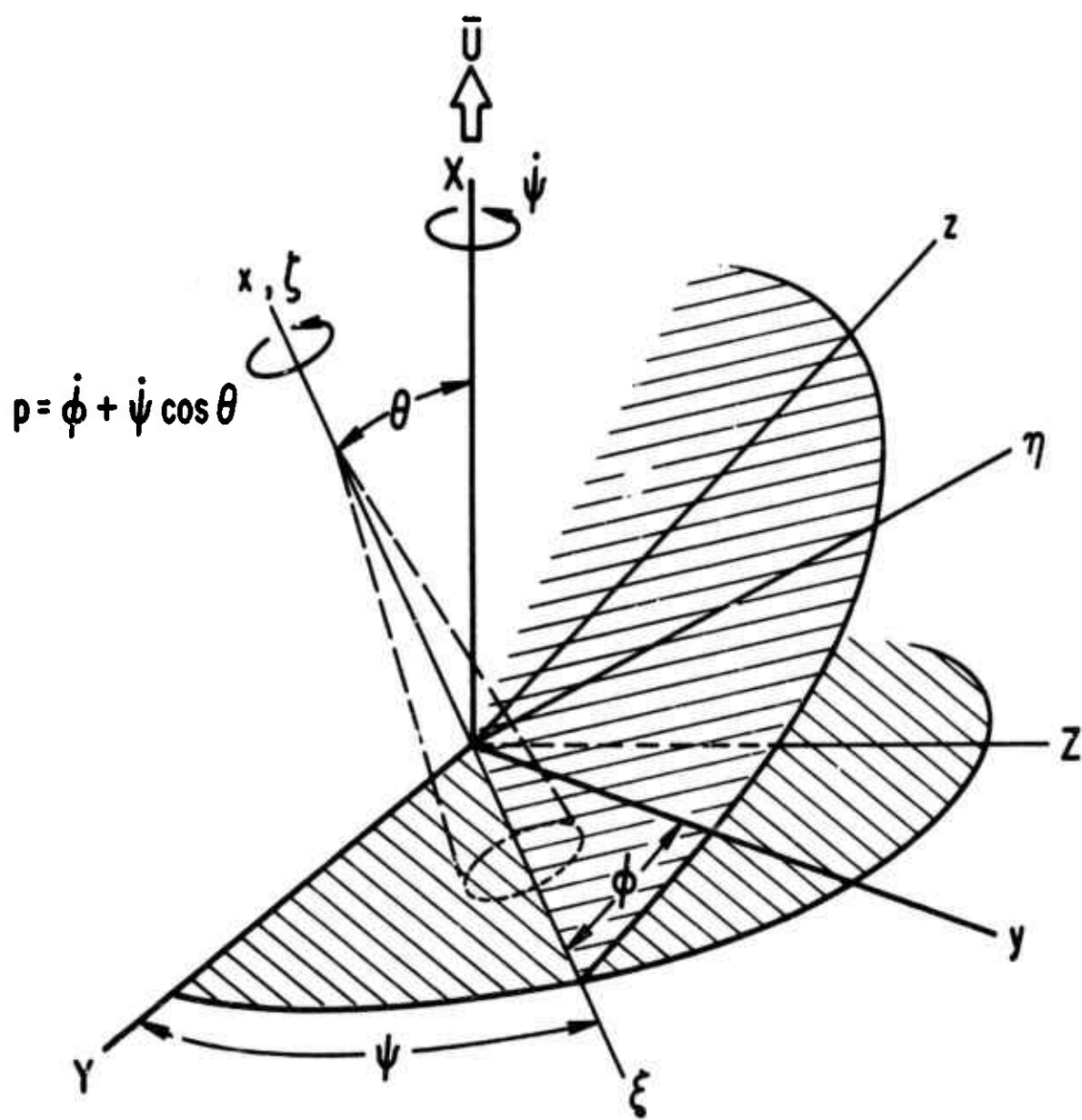
Figure 1. Euler Angles for Three-Degree-of-Freedom
Rotational Motion

$$M_\xi = -C_{N_\alpha} qS\ell\theta - \frac{qSd^2}{2u}\left[-C_{m_q} + \frac{2C_{N_\alpha} I}{md^2}\right]\dot\theta$$

$$M_\eta = \frac{qSd^2}{2u}\left[C_{m_q} - \frac{2C_{N_\alpha} I}{md^2}\right]\dot\psi \sin\theta \qquad (3)$$

$$M_\zeta = C_\ell qSd$$

where ℓ is the vehicle static margin (considered positive for the statically stable vehicle), and the damping terms consist of both the pitch (or yaw) damping derivative C_{m_q} plus a normal force damping term $2C_{N_\alpha} I/md^2$ to account for lateral motion of the vehicle center of mass.[*]

Substituting Eq. (3) in Eq. (1) and dividing the first two equations by I and the third by I_x gives

$$-\omega^2\theta - \nu\dot\theta = \ddot\theta + \mu p\dot\psi \sin\theta - \dot\psi^2 \sin\theta \cos\theta$$

$$-\nu\dot\psi \sin\theta = \frac{d}{dt}(\dot\psi \sin\theta) + \dot\theta\dot\psi \cos\theta - \mu p\dot\theta \qquad (4)$$

$$\kappa = \dot p$$

where the coefficients are

$$\omega^2 = \frac{C_{N_\alpha} qS\ell}{I} \qquad\qquad \kappa = \frac{C_\ell qSd}{I_x}$$

$$\qquad (5)$$

$$\nu = \frac{qSd^2}{2Iu}\left(-C_{m_q} + \frac{2C_{N_\alpha} I}{md^2}\right) \qquad \mu = \frac{I_x}{I}$$

The parameter ω is the natural pitch frequency of the vehicle.

---

[*] It can be shown, for an axisymmetric vehicle, that the lateral motions of the center of mass from normal forces acting at the center of pressure are proportional to pitch or yaw rotations about a point a distance $I/m\ell$ ahead of the center of mass.

III. QUASI-STEADY SOLUTION FOR ANGLE-OF-ATTACK CONVERGENCE

The vehicle motion during reentry, described in terms of the time-dependent Euler angles $[\Psi(t), \phi(t), \theta(t)]$, is assumed to be of the form

$$[\Psi(t), \phi(t), \theta(t)] = [\overline{\Psi}(t), \overline{\phi}(t), \overline{\theta}(t)] + [\Psi_+(t), \phi_+(t), \theta_+(t)] \qquad (6)$$

where $[\overline{\Psi}(t), \overline{\phi}(t), \overline{\theta}(t)]$ represents a quasi-steady component that varies relatively slowly with time (of the order of the dynamic pressure) and $[\Psi_+(t), \phi_+(t), \theta_+(t)]$ represents an oscillation of higher frequency about the average (quasi-steady) values. In the ensuing analysis, the oscillations are neglected and a solution is obtained for the quasi-steady angle-of-attack convergence behavior of the descending vehicle. This development is heuristic in nature and based on physical intuition. It is justified on the basis of agreement with more complete and lengthier analyses presented later.

Taking $\sin\theta \approx \theta$ and $\cos\theta \approx 1$ and neglecting pitch damping ν in the first of Eqs. (4) gives, for the pitch equation,

$$\ddot{\theta} + (\omega^2 + \mu p\dot{\Psi} - \dot{\Psi}^2)\,\theta = 0 \qquad (7)$$

This equation describes a nonlinear oscillation in θ about a nonzero quasi-steady value $\overline{\theta}$, since θ, by definition, is always positive. One can interpret the corresponding quasi-steady values of $\overline{\Psi}$ to be those that make $\ddot{\theta}$ in Eq. (7) zero, thus satisfying the relation

$$\omega^2 + \mu p\overline{\Psi} - \overline{\Psi}^2 = 0$$

or

$$\overline{\Psi} = (\mu p/2) \pm \left[(\mu p/2)^2 + \omega^2\right]^{1/2} \qquad (8)$$

This result is valid as long as θ is appreciably greater than the trim angle of attack from aerodynamic or mass asymmetries (assumed to be zero for the present analysis). For $\mu p/2$ small relative to ω, the two values for $\overline{\dot{\psi}}$ may be written approximately

$$\overline{\dot{\psi}} = \omega + \frac{\mu p}{2}, \qquad -\omega + \frac{\mu p}{2} \tag{9}$$

This indicates that, for values of angle of attack sufficiently greater than trim, the precession rate $\dot{\psi}$ can oscillate in either a positive or negative mode, the quasi-steady value of which is slightly displaced from the natural pitch frequency for a slender vehicle, as shown in Fig. 2.[*] The mode of oscillation depends on the initial reentry conditions and is discussed later. Once $\dot{\psi}$ is determined, the windward-meridian rotation $\dot{\phi}$, for small θ, is simply the difference between the roll rate p (assumed known) and $\dot{\psi}$.

The angle-of-attack convergence can be obtained from the second of Eqs. (4). This equation can be written

$$\frac{d}{dt} (\dot{\psi} \sin^2\theta) + \nu\dot{\psi} \sin^2\theta - \mu p\dot{\theta} \sin\theta = 0 \tag{10}$$

which, for small θ, can be differentiated to give

$$\left(\dot{\psi} - \frac{\mu p}{2}\right) \frac{d}{dt}\left(\theta^2\right) + \left(\frac{d\dot{\psi}}{dt} + \nu\dot{\psi}\right)\theta^2 = 0. \tag{11}$$

---

[*] The two precession modes, Eqs. (8) or (9), are analogous to the fast and slow precession of a spinning top but differ in sign, because the pitch moment acts in the opposite direction to the top turning moment for a statically stable missile.
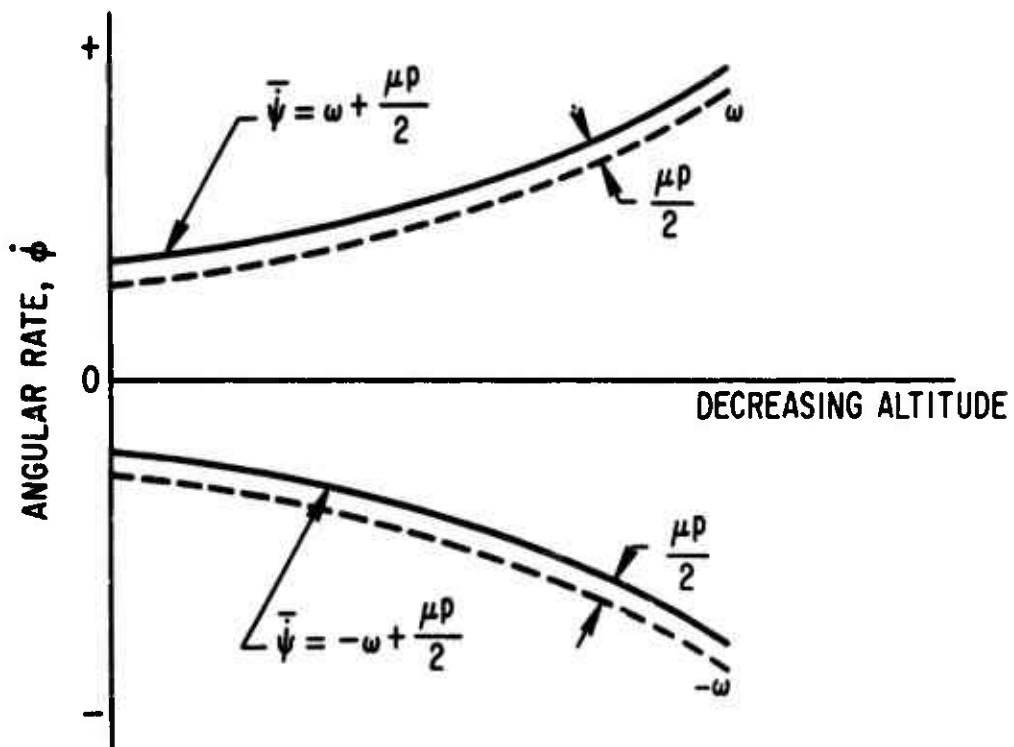
-8-

Figure 2.   Precession Modes

We now consider the time variation of the quasi-steady values $\overline{\theta}$ and $\overline{\dot{\psi}}$ by writing Eq. (11) in the form

$$\frac{d}{dt}\overline{\theta}^2 + f(t)\overline{\theta}^2 = 0, \qquad (12)$$

where

$$f(t) \equiv \frac{(d\overline{\dot{\psi}}/dt) + \nu\overline{\dot{\psi}}}{\overline{\dot{\psi}} - (\mu p/2)} \qquad (13)$$

Equation (12) has the familiar solution

$$\left(\frac{\overline{\theta}}{\theta_o}\right)^2 = \exp\left(-\int_o^t f(t')dt'\right). \qquad (14)$$

On substituting $\overline{\dot{\psi}}$ from Eq. (8) in Eq. (13) and integrating this result in Eq. (14) we find, for the quasi-steady angle-of-attack convergence, the expression

$$\frac{\overline{\theta}}{\theta_o} = (1 + \sigma^2)^{-1/4} \exp\left\{-\frac{1}{2}\int_o^t \left(\frac{\dot{p}}{p} + \nu\right)\left[1 \pm (1 + \sigma^2)^{-1/2}\right]dt\right\} \qquad (15)$$

where $\sigma \equiv 2\omega/\mu p$. The plus and minus signs in the exponent correspond to the positive and negative modes, respectively, of the precession rate $\dot{\psi}$, depicted in Fig. 2. The roll acceleration term $\dot{p}/p$ in the exponent is an effective damping term that adds to or subtracts from the damping coefficient ν, depending on the sense of the roll acceleration.[*] Similarly, the term $(1 + \sigma^2)^{-1/2}$

---

[*] It appears that negative (decelerating) values of $\dot{p}$ that yield negative values for the effective damping coefficient $[(\dot{p}/p) + \nu]$ would produce a momentary angle-of-attack divergence. Such cases might prove interesting for future investigations.

either increases or decreases the effective damping and, therefore, increases or decreases the rate of angle-of-attack convergence, depending on whether the precession mode is positive or negative. The conditions that determine the precession mode are discussed later.

For a slender reentry vehicle, $\mu \ll i$, the parameter σ^2 is generally much greater than unity except for highly supercritical roll rates $p \gg \omega$. Therefore, in most cases the term $(i + \sigma^2)^{-1/2}$ in the exponent of Eq. (15) can be ignored compared with unity, and Eq. (15), with the assumption $1 + \sigma^2 \approx \sigma^2$, reduces to

$$\frac{\overline{\theta}}{\theta_o} = \left(\frac{\mu P_o}{2\omega}\right)^{1/2} \exp\left[-\frac{1}{2}\int_o^t \nu \, dt\right]. \tag{16}$$

For an exponential atmosphere of scale height H, and with a straight-line trajectory of path angle γ, the integral of Eq. (16) can be evaluated and the angle-of-attack convergence ratio reduces to the simple result

$$\frac{\overline{\theta}}{\theta_o} = \left(\frac{\mu P_o}{2\omega}\right)^{i/2} e^{-bp}, \tag{17}$$

where

$$b = \frac{H S d^2}{8I \sin \gamma}\left(-C_{m_q} + \frac{2C_{N_\alpha} I}{md^2}\right) \tag{18}$$

and ρ is density. The results, Eq. (16) or (17), indicate that for roll rates that are not excessively supercritical [i.e., for $(i + \sigma^2)^{-1/2} \ll i)$], the angle-of-attack convergence depends only on the reentry roll rate and is independent of roll acceleration.

For the constant roll rate case ($\dot{p} = o$), the result, Eq. (15), reduces to an expression similar to that derived in Ref. 1 for the negative precession mode.

IV. INITIAL REENTRY CONDITIONS

Before reentry, the vehicle is in a state of moment-free motion, and the relation between the various angular rates is uniquely determined. In general, the vehicle will have some initial roll rate p_o and will undergo a steady precession (coning motion) with a precession rate Ω and cone half-angle α (Fig. 3). The cone axis will, in general, be inclined to the flight path, and the velocity vector may lie inside or outside the coning circle. The latter case is shown in Fig. 3. The exoatmospheric roll rate, precession rate, and cone half-angle are related by the expression

$$\Omega = \frac{\mu p_o}{\cos \alpha} \tag{19}$$

This relation follows from the first of Eqs. (4) with $\dot{\theta} = \ddot{\theta} = \omega = o$, and α and Ω substituted for θ and $\dot{\psi}$, respectively.

After entering the atmosphere, the statically stable vehicle is subjected to an aerodynamic pitch moment that tends to align the vehicle with the flight path. However, because of the angular momentum comprised of the roll and precession rates, which, on the average, is directed along the coning axis, the pitch motion is resisted by gyroscopic forces that induce a precession of the angular momentum vector about the average flight path. This precession is opposite in direction to the angular momentum (retrograde precession). A projection of the path described would be as shown in Fig. 4 when viewed along the direction of flight. The residual coning motion, in the same direction as the angular momentum vector (e.g., clockwise), has been called nutation by Nicolaides,[7] and the retrograde precession in the opposite direction (counter-clockwise) has been called, simply, precession.[*] In general, the two motions exist simultaneously.

---

[*] These definitions are more restrictive than are the classical definitions of nutation and precession as being variations in θ and ψ, respectively (see, for example, Ref. 8, p. 432).
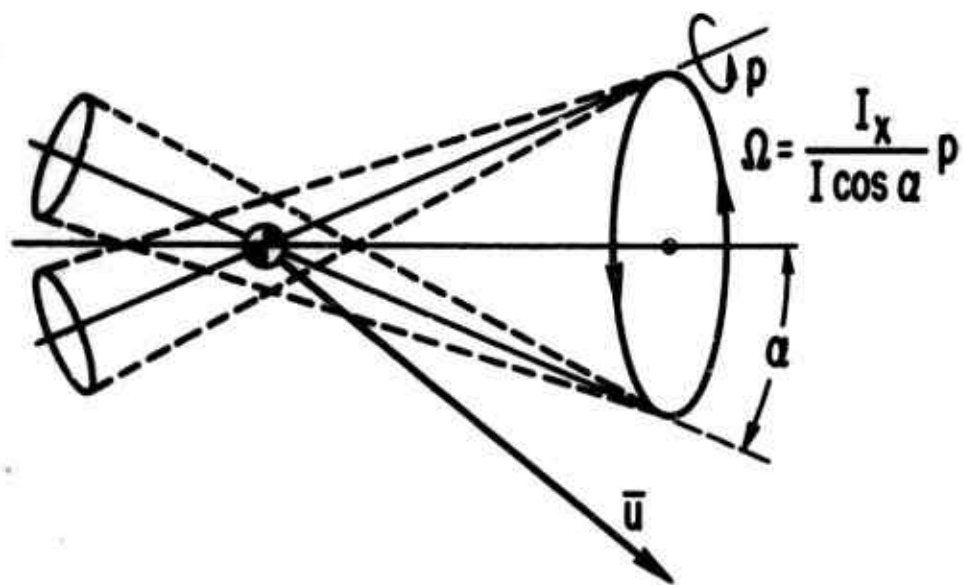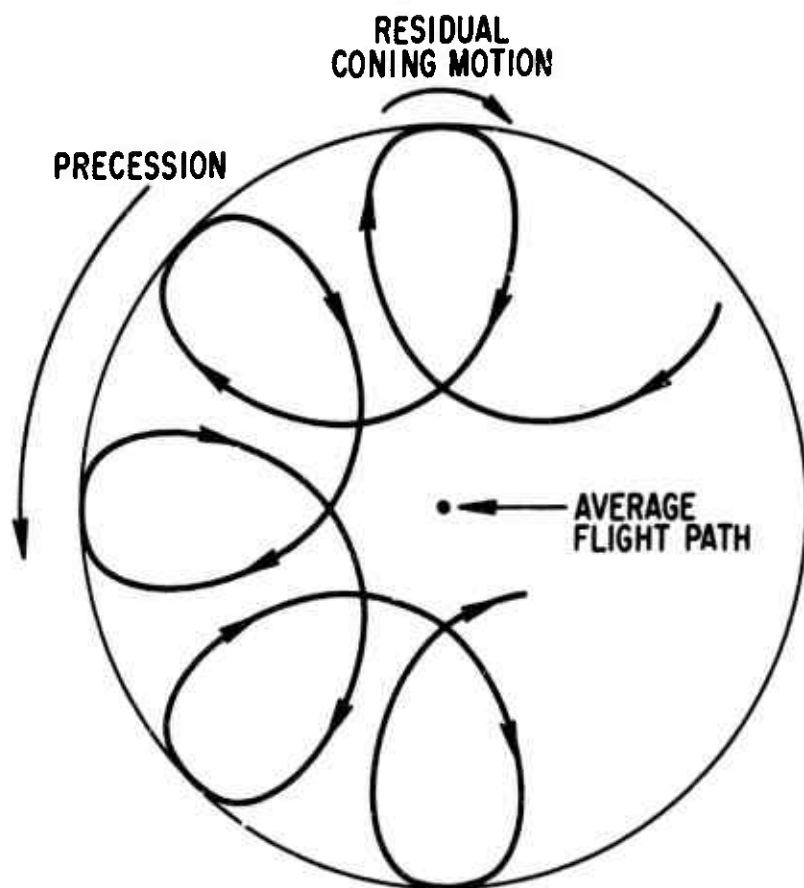
Figure 3. Exoatmospheric Motion

Figure 4. Retrograde Precession

The expression derived above for angle-of-attack convergence, Eq. (15), corresponds to two limiting cases of the type of motion depicted in Figs. 3 and 4. The first case, with the negative sign in the exponent, represents the limiting condition of zero coning half-angle for which the vehicle is initially at angle of attack with respect to the flight path and is rolling, as shown in Fig. 5a. The second case, with the positive sign in the exponent, is the condition in which the axis of the initial coning motion coincides with the average flight path, as shown in Fig. 5b.

The Euler angles (Ψ, ϕ, θ) were defined with respect to an inertial frame of reference that moves along the flight path such that $\dot{\Psi}$ represents precession about the velocity vector (Fig. 1). Therefore, the two exoatmospheric conditions represented in Figs. 5a and 5b correspond to initial conditions on $\dot{\Psi}$ of $\dot{\Psi}_0 = 0$ and $\dot{\Psi}_0 = \Omega = \mu p_0 / \cos \theta_0$, respectively. Referring back to the quasi-steady solution for $\dot{\Psi}$, Eq. (8), we note that, in the limit as $\omega \to 0$, corresponding to zero atmospheric density, $\overline{\dot{\Psi}}$ can have the two values 0 and μp (the latter value would be $\mu p / \cos \theta$, without the small angle approximations in Eq. 7). Therefore, the two precession modes shown in Fig. 2 follow from the two cases of exoatmospheric motion shown in Fig. 5. Under certain conditions when the initial precession mode is positive, an instability can occur in the presence of roll acceleration whereby the motion changes from the positive to the negative precession mode. A criterion for predicting this instability is derived in the next section.
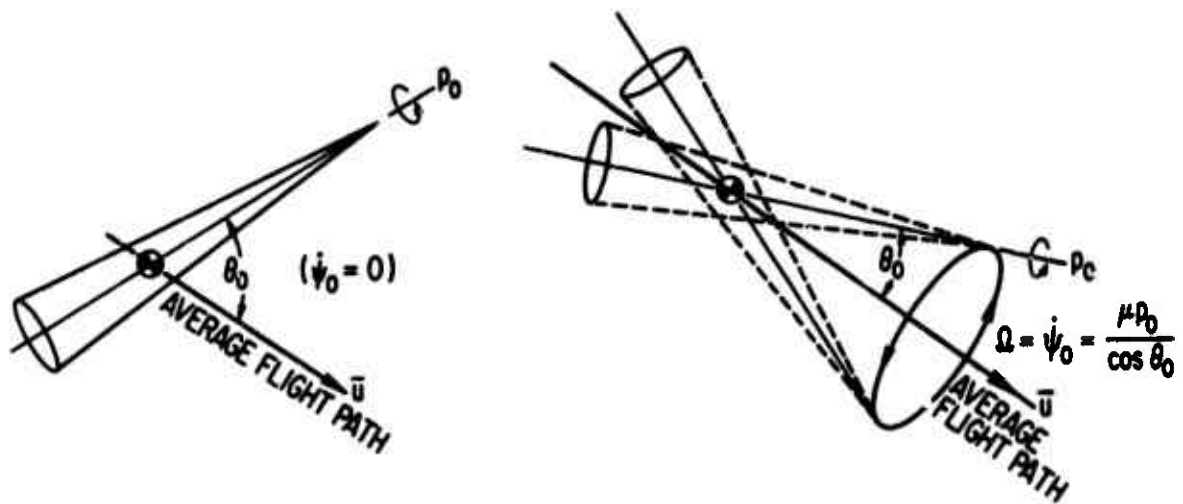
Figure 5. Limiting Cases of Exoatmospheric Motion

V. PRECESSION INSTABILITY

Equation (11) describes the relation between the total angle of attack θ and the precession rate $\dot{\psi}$, without any assumption of quasi-steady motion. This equation can be written in the form

$$\dot{\theta} = -\frac{(d\dot{\psi}/dt) + \nu\dot{\psi}}{2\dot{\psi} - \mu p}\theta \tag{20}$$

which reveals much about the vehicle motion. First, we note that θ, by definition, is always positive and $\dot{\psi}$, from the above considerations, oscillates about either the positive or the negative branch of the natural pitch frequency curve ω, as shown in Fig. 2. Therefore, for $\dot{\psi} > \mu p/2$, the denominator of Eq. (20) remains positive, and, for small damping, $d\theta/dt = 0$ at approximately $d\dot{\psi}/dt = 0$, so that θ and $\dot{\psi}$ oscillate at the same frequency with the θ maxima corresponding to the $\dot{\psi}$ minima and vice versa. Similarly, for $\dot{\psi} < \mu p/2$, the maxima and minima of both θ and $\dot{\psi}$ are in phase, as shown in Fig. 6. These results can be deduced in another manner. Equation (10), with the assumptions $\nu = 0$ and $\sin\theta \approx \theta$, can be written in the form

$$\frac{d}{dt}(\dot{\psi}\theta^2) - \frac{\mu p}{2}\frac{d}{dt}(\theta^2) = 0 \tag{21}$$

With the further assumption that p is constant (or slowly varying relative to the θ or $\dot{\psi}$ oscillations), Eq. (21) can be integrated to give

$$(\dot{\psi} - \frac{\mu p}{2})\theta^2 = \text{constant} \tag{22}$$

Equation (22), being the first integral of an equation of motion, is an energy expression and indicates that $|\dot{\psi} - (\mu p/2)|$ is maximum for θ minimum and vice versa, as depicted in Fig. 6. However, if $\dot{\psi}$ is in the positive mode such
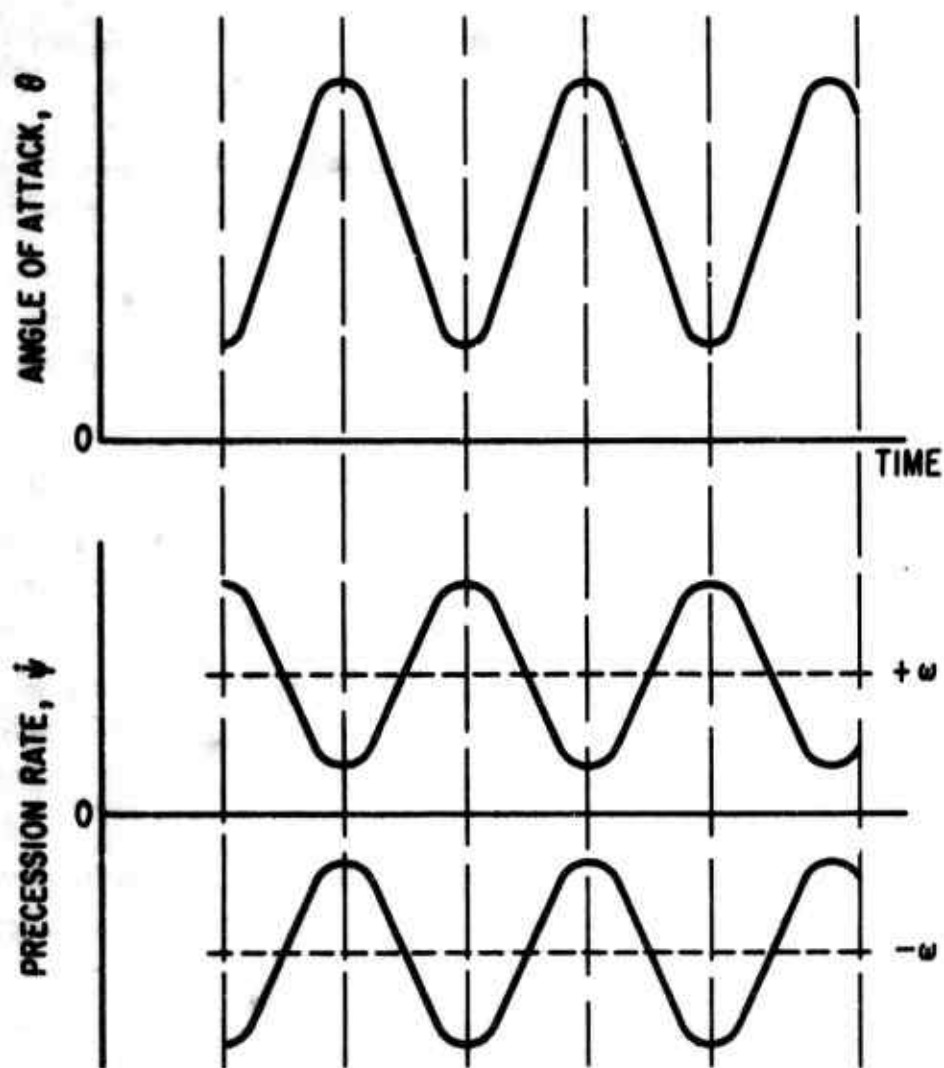
Figure 6. Angle-of-Attack and Precession Rate
Oscillation Behavior

that $\dot\psi > \mu p/2$, and p increases because of an applied roll torque, an instability will occur as $\mu p/2$ approaches the minimum value of the $\dot\psi$ oscillation, which causes the denominator of Eq. (20) to approach zero. It is shown from a phase plane analysis, which follows, that at the point of instability the $\dot\psi$ oscillation diverges without limit and finally reverses sign from an infinitely large positive upper bound to an infinitely large negative lower bound. Thereafter, $\dot\psi$ remains in the more stable negative mode. The divergence in $\dot\psi$ corresponds to a lower bound on the θ oscillation that approaches zero, from Eq. (22).

Equations (7) and (20) can be combined to give a single equation in $\dot\psi$

$$2\left(\dot\psi - \frac{\mu p}{2}\right)\left(\frac{d^2\dot\psi}{dt^2} + \nu\frac{d\dot\psi}{dt} + \dot\nu\dot\psi\right) - 3\left(\frac{d\dot\psi}{dt}\right)^2 + (\mu\dot p - 4\nu\dot\psi)\frac{d\dot\psi}{dt} + \mu\nu\dot p\dot\psi$$

$$- \nu^2\dot\psi^2 = 4\left(\dot\psi - \frac{\mu p}{2}\right)^2 (\omega^2 + \mu p\dot\psi - \dot\psi^2). \tag{23}$$

We can put this equation in a form suitable for phase plane analysis by making the substitutions

$$y \equiv \dot\psi - \frac{\mu p}{2}$$

$$v \equiv \dot y = \frac{d\dot\psi}{dt} - \frac{\mu}{2}\dot p \tag{24}$$

$$v\frac{dv}{dy} = \ddot y \quad \frac{d^2\dot\psi}{dt^2}$$

in which $\dot{p}$ has been assumed to be negligible. Equation (23) is then written

$$\frac{dv}{dy} = \frac{-2y^2(y^2 - a^2) + cy(y + d) + (3/2)v(v + b) + \nu v y}{yv},$$ (25)

where

$$a \equiv \left[\omega^2 + (\mu p/2)^2\right]^{1/2}$$

$$b \equiv (2/3)\mu (\dot{p} + \nu p)$$ (26)

$$c \equiv (1/2)(\nu^2 - 2\dot{\nu})$$

$$d \equiv \mu p \frac{\nu^2 - \dot{\nu}}{\nu^2 - 2\dot{\nu}}$$

The parameters a, b, c, d, and ν vary slowly with time (of the order of the dynamic pressure) relative to y and are assumed to be constants in the ensuing analysis. The stability conditions so obtained from a phase plane evaluation of Eq. (25) apply at any instant of time with the appropriate values of these parameters. However, since these parameters do change with time, the nature of the motion and the stability criteria change accordingly. This is discussed in greater detail later.

Singularities in the v - y plane (points where the right side of Eq. (25) takes the form zero over zero) are seen to occur at

$$y = 0 \quad , \quad v = 0$$

$$y = 0 \quad , \quad v = -b$$

$$y = y_1 \quad , \quad v = 0$$

$$y = y_2 \quad , \quad v = 0$$

$$y = y_3 \quad , \quad v = 0$$

-22-

where y_1, y_2, and y_3 are roots of

$$y^3 - \left(a^2 + \frac{c}{2}\right)y - \frac{cd}{2} = 0. \tag{27}$$

The parameters c and d are, in general, much smaller than a^2, and the roots of Eq. (27) can be shown to be approximately given by

$$y_1 \approx a + \epsilon + \frac{\epsilon d}{a[1+(\epsilon/a)]^2}$$

$$y_2 \approx -a - \epsilon + \frac{\epsilon d}{a[1+(\epsilon/a)]^2} \tag{28}$$

$$y_3 \approx \frac{-2\epsilon d}{a[1+(\epsilon/a)]^2}$$

where ϵ is small relative to a and is defined by

$$\epsilon \equiv \frac{c}{4a} = \frac{(v^2 - 2\dot{v})}{8[\omega^2 + (\mu p/2)^2]^{1/2}} \tag{29}$$

We now examine the character of each singularity in order to construct the solution curves to the equation of motion. Equation (25) can be written in the approximate form

$$\frac{dv}{dy} = \frac{-2y(y-a)(y+a)[y+(2\epsilon d/a)] + \frac{3}{2}v(v+b) + vvy}{yv} \tag{30}$$

in which the terms containing ϵ have been neglected relative to a, since they do not change the character of the singularity. Consider first the singularity at $y = a$, $v = 0$. If the origin is shifted to the singularity with the substitution $x = y - a$, the slope dv/dx in the limit as x, $v \to 0$ is found to be of the form

$$\lim_{\substack{x \to 0 \\ v \to 0}} \frac{dv}{dx} = \frac{-4a^2 x + \left[(3b/2a) + v\right]v}{v} \qquad (31)$$

Equation (31) is a special case of the differential equation

$$\frac{dv}{dx} = \frac{Ax + Bv}{Cx + Dv} \qquad (32)$$

which has the characteristic equation

$$\lambda^2 - \lambda(B + C) - (AD - BC) = 0. \qquad (33)$$

The nature of the singularities is determined by the relative magnitudes of the constants A, B, C, and D, and the various singularities that can arise from Eq. (32) have been previously investigated. Table 1[9] characterizes these singularities. The singularity at $y = a$, $v = 0$ described by Eq. (31) is characterized by the coefficients

Table 1. Characteristics of the Singularities of $\frac{dv}{dx} = \frac{Ax + Bv}{Cx + Dv}$

$(B - C)^2 + 4AD > 0$	Node if $AD - BC < 0$ Saddle if $AD - BC > 0$	$\begin{cases}\text{Stable if } B + C < 0 \\ \text{Unstable if } B + C > 0\end{cases}$
$(B - C)^2 + 4AD < 0$	Center if $B + C = 0$ Spiral if $B + C \neq 0$	$\begin{cases}\text{Stable if } B + C < 0 \\ \text{Unstable if } B + C > 0\end{cases}$
$(B - C)^2 + 4AD = 0$	Node	$\begin{cases}\text{Stable if } B + C < 0 \\ \text{Unstable if } B + C > 0\end{cases}$

$$A = -4a^2 \qquad C = 0$$
$$B = \frac{3b}{2a} + v \qquad D = 1,$$

in which the constants a, b, and v are positive by definition. For this case, $(B - C)^2 + 4AD = [(3b/2a) + v]^2 - 16a^2 < 0$ (since $\frac{b}{a}$, $v \ll a$) and $B + C = (3b/2a) + v > 0$. Therefore, the singularity is an unstable spiral. Similarly, for the singularity at $y = -a$, $v = 0$, if the origin is shifted to the singularity with the substitution $x = y + a$, the limiting value of the slope dv/dx is found to be

$$\lim_{\substack{x \to 0 \\ v \to 0}} \frac{dv}{dx} = \frac{-4a^2 x - [(3b/2a) - v]v}{v} \qquad (34)$$

For this case, $(B - C)^2 + 4AD = [(3b/2a) + v]^2 - 16a^2 < 0$, as before, but $B + C = -(3b/2a) + v$, which may be greater or less than zero, depending on the damping and roll acceleration. Therefore, this singularity is either a stable or unstable spiral.

The quantity $B + C$, which determines the degree of stability or instability of the spiral singularities at $\pm a$, 0 is proportional to the pitch damping and roll acceleration, which are, in general, small quantities. For the case of zero damping and constant roll rate (i.e., $v = \dot{p} = 0$), then $B + C = 0$ and the spiral singularities reduce to center-type singularities in this limiting case. The singularities at $\pm a$, 0 therefore signify the existence of either stable or quasi-stable oscillations in y about the equilibrium values $y = \pm a$, depending on the magnitude of pitch damping and roll acceleration. Moreover, the oscillations about $y = +a$ are of either constant or diverging amplitude, corresponding to the center or unstable spiral singularities, whereas the oscillations about $y = -a$ may be either of constant, diverging, or converging amplitude, depending on the relative magnitudes of the pitch damping and roll acceleration. From the definition of y, Eq. (24), the oscillations in y about

-25-

±a correspond to the direct and retrograde precession oscillations in $\dot{\psi}$ about the positive and negative branches, respectively, of the natural pitch frequency curves identified earlier in Fig. 2.

The above considerations are based on the assumption of quasi-steady motion for which the parameters defined by Eq. (26) were assumed to be constants. However, since these parameters change slowly with time, they influence the character of the motion. Consider, for example, the oscillation in y about the singularity y = +a and let there be a positive roll acceleration so that the roll rate p increases with time. The increase in p reduces y, from the definition, Eq. (24), whereas the value a about which y oscillates increases approximately as the natural pitch frequency. The net effect is to increase the amplitude of the oscillation; this increase is characteristic of the unstable spiral singularity that exists at y = +a with the presence of a roll acceleration. It will be shown that if p increases sufficiently to drive y to zero (i.e., μp/2 approaches the minimum value of $\dot{\psi}$), an instability occurs whereby the motion reverses from an oscillation about y = +a to a more stable oscillation about y = -a. The nature of the crossover becomes apparent from the character of the remaining singularities at and near the origin.

Consider the singularity at y = 0, v = -b. The origin is shifted to the singularity by the substitution w = v + b. The slope dw/dy in the limit as y, w→0 is

$$\lim_{\substack{y \to 0 \\ w \to 0}} \frac{dw}{dy} = \frac{[v - (4\epsilon ad/b)]\, y + \frac{3}{2}w}{y} \tag{35}$$

This singularity is characterized by $(B - C)^2 + 4AD = 1/4 > 0$, AD - BC = - 3/2 < 0 and B + C = 5/2 > 0, which is an unstable node. For the singularity y = - (2ϵd/a), the origin is shifted to the singularity with the substitution x = y + (2ϵd/a) and the limiting slope is

$$\lim_{\substack{x \to 0 \\ v \to 0}} \frac{dv}{dx} = \frac{2a^2 x - [(3ab/4\epsilon d) - \nu] v}{v} \tag{36}$$

The characteristic values are $(B - C)^2 + 4AD = [(3ab/4\epsilon d) - \nu]^2 + 8a^2 > 0$ and $AD - BC = 2a^2 > 0$. Therefore, the singularity is a saddle. Finally, the singularity at the origin, $y = 0$, $v = 0$, has the limiting slope

$$\lim_{\substack{y \to 0 \\ v \to 0}} \frac{dv}{dy} = \frac{4ad\epsilon y + (3/2) bv + \nu \, yv}{yv}. \tag{37}$$

This is a higher-order singularity than those characterized by Eq. (32), and the nature of the singularity is not readily determined analytically. Consequently, a numerical technique such as the method of isoclines[10] is required for determining the behavior of the solution curves in the neighborhood of the singularity.

Figure 7 summarizes, schematically, the character of the four singularities analyzed above plus the higher-order singularity at the origin deduced from limiting cases of Eq. (37). The relative spacing between the singularities is grossly distorted, since ϵ is, in general, a very small quantity compared with a. The qualitative behavior of the solution curves in the neighborhood of the singularities near the origin, as determined from a plot of Eq. (25) by the method of isoclines, is shown in Fig. 8. The nature of the crossover from an oscillation about the positive branch of the pitch frequency curve to an oscillation about the negative branch now becomes apparent. Figure 8 shows that there are two switching lines in the positive halfplane and one in the negative halfplane. To the right of the first switching line, an oscillation about the positive branch persists until the amplitude reaches sufficient magnitude to reach the first switching line as $y \to 0$. It then appears possible to follow a trajectory between the two switching lines which will pass through the singularities but continue around the positive branch (trajectories labeled 3 and 4). Beyond the second switching line the trajectory loops around the negative
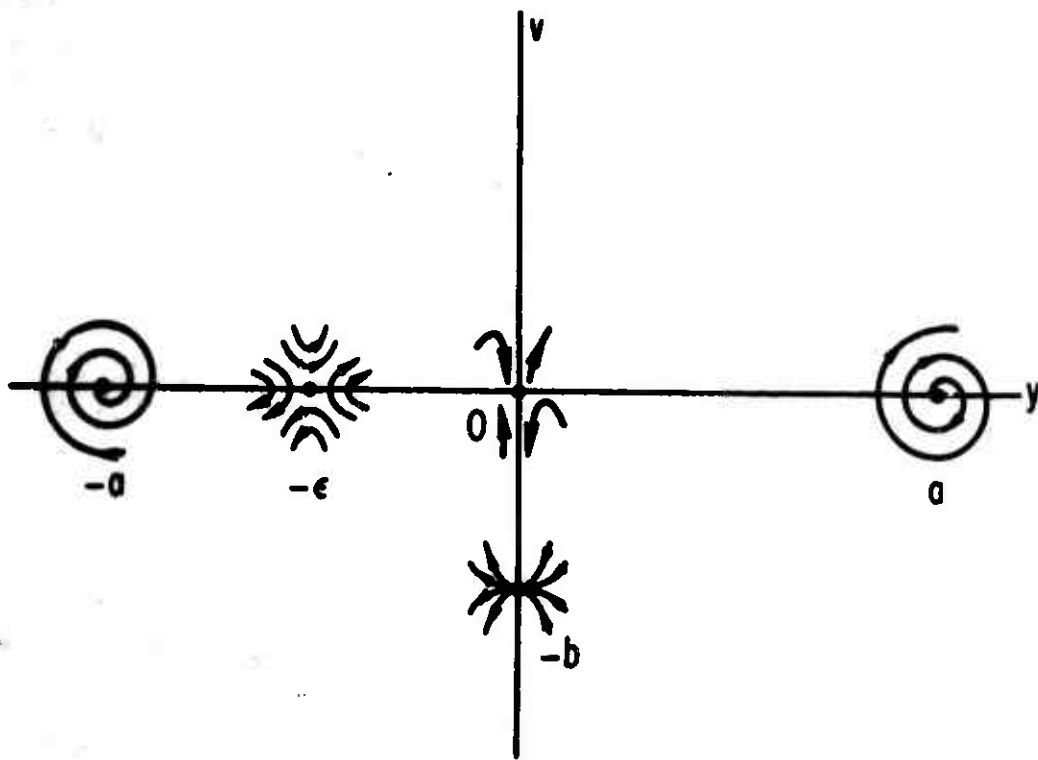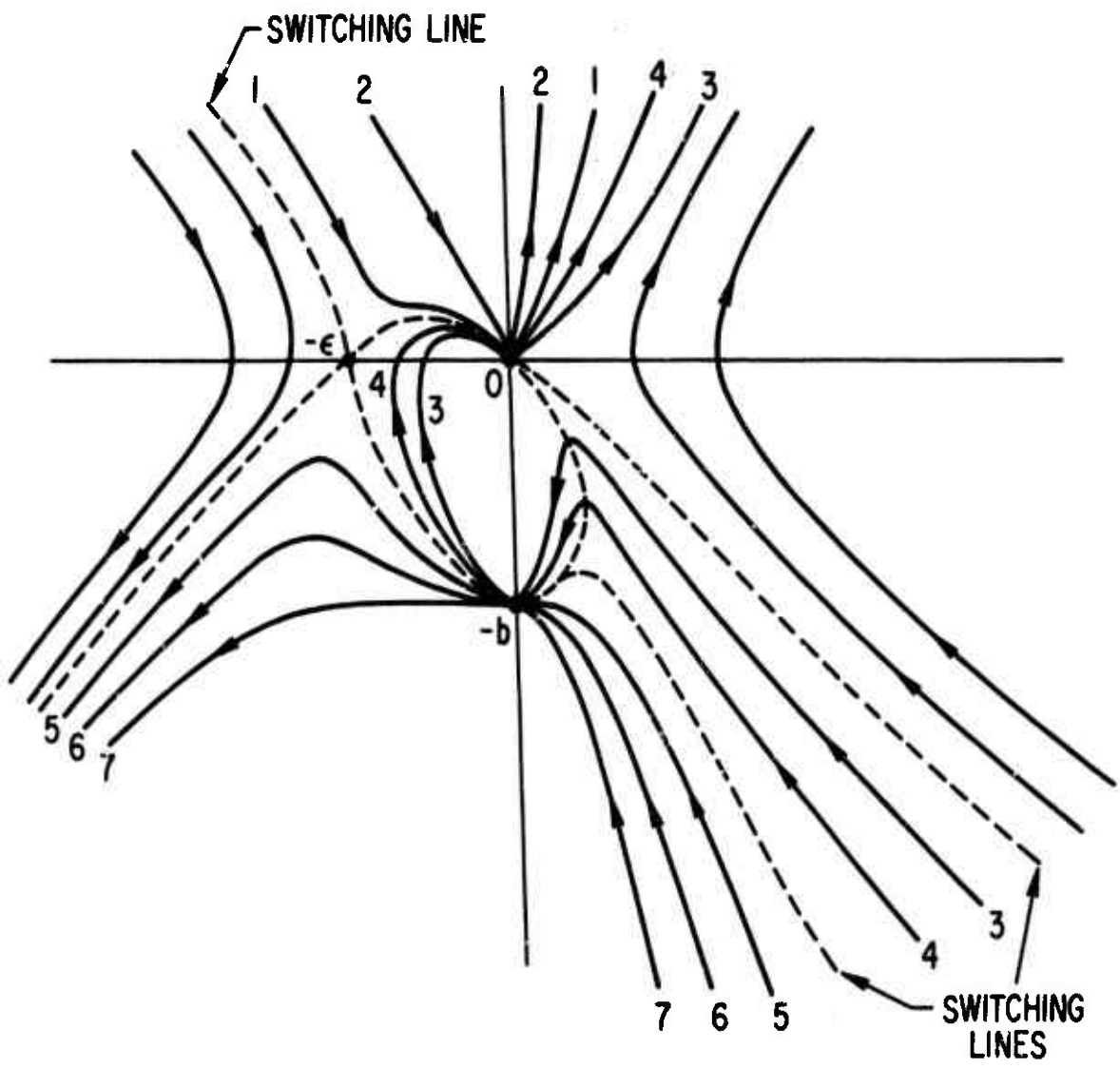
-27-

Figure 7. Singularities in Phase Plane

Figure 8. Solution Curves in Neighborhood of Origin

branch (y = -a) and can return to the positive branch provided it passes to the right of the switching line in the negative halfplane (trajectories 1 and 2). This motion through the singularities at the origin represents a brief period of instability, which occurs only at the instant y → 0. As was pointed out earlier, the spacing between the singularities in the vicinity of the origin is extremely small compared with the amplitude of the motion. Also, in view of the decreasing value of y due to the increase in roll rate, it would be expected that only a small number of trajectories, if any, would pass through this region. To the left of the origin, as y continues to decrease due to the increasing roll rate, the oscillations appear to become more stable about the negative branch, as represented by the trajectories to the left of the singularity at -ε. This behavior has been verified by computer solutions of the equations of motion, which are discussed later.

Some further insight can be obtained from a physical interpretation of the relation, Eq. (20), between the angle of attack and the precession rate. From the definition for y, Eq. (24), the limiting case y = 0 corresponds to a zero value of the denominator on the right side of Eq. (20). But since θ, by definition, is always positive, this would represent an instability in θ (i.e., a large value of $\dot{\theta}$) unless either θ or $(d\dot{\psi}/dt) + \nu\dot{\psi}$ also approached zero along with y. What is found from the computer solutions is that θ does approach zero in the region of instability, since the θ oscillations are coupled with the $\dot{\psi}$ oscillations through Eq. (22), as depicted in Fig. 6. From conservation of energy, as θ approaches its minimum $|\dot{\psi} - (\mu p/2)|$ approaches its maximum and vice versa. Therefore, the extreme values of $\dot{\psi}$ (or y), both positive and negative, will occur in the region of instability as y → 0. This is shown qualitatively in Fig. 9.

The foregoing discussion has dealt with the precession rate $\dot{\psi}$, which is related to the roll rate p and the windward-meridian rotation rate $\dot{\phi}$ through the relation, Eq. (2),

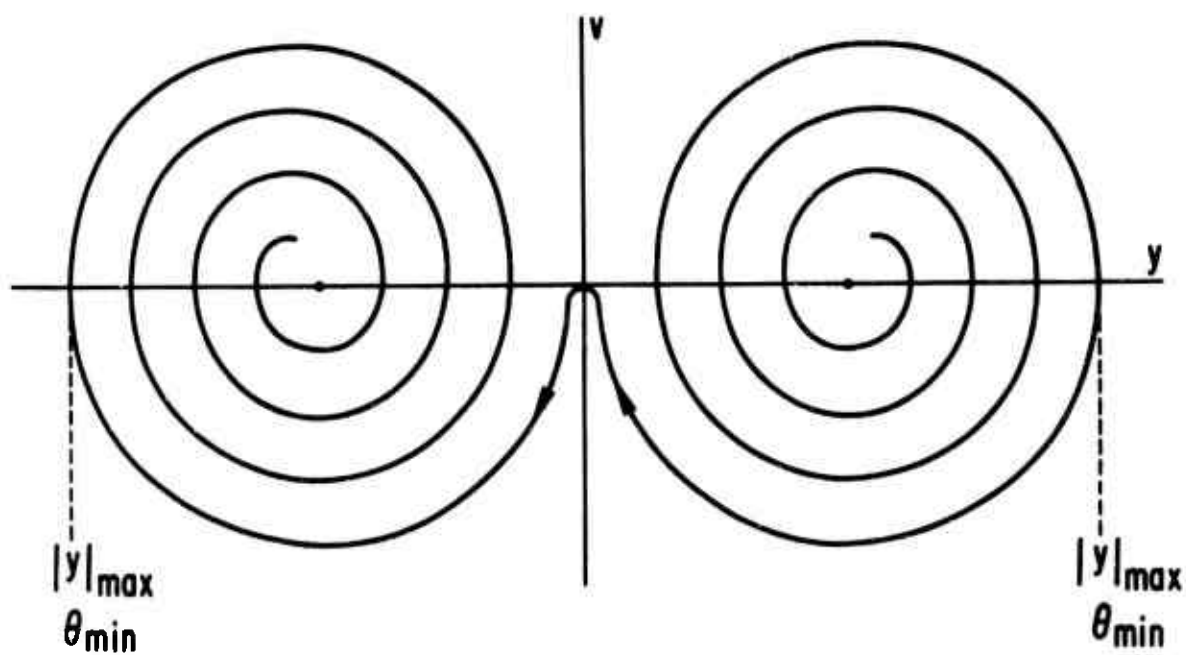$$p = \dot{\phi} + \dot{\psi} \cos \theta \quad , \tag{2}$$

-30-

Figure 9.   Qualitative Behavior of Solution Curves in Phase Plane

or, for small θ,

$$p \approx \dot{\phi} + \dot{\psi} \qquad . \qquad (38)$$

From the third of Eqs. (4), the roll rate is gyroscopically uncoupled from the other angular rates and depends only on the roll moment coefficient. Therefore, for a prescribed roll history, the windward-meridian rotation rate is simply the difference $\dot{\phi} = p - \dot{\psi}$. Depending on the roll history and on whether $\dot{\psi}$ is in the positive or negative mode, the windward meridian may be either "oscillatory" or "rotary"; i.e., the vehicle either oscillates about its roll axis relative to the wind or rotates continuously in one direction. This is illustrated in Fig. 10 for an arbitrary roll rate history. When $\dot{\psi}$ is in the positive mode with the roll history shown, $\dot{\phi}$ oscillates from positive to negative with the quasi-steady value $\bar{\dot{\phi}} = p - \omega - \epsilon$. However, for $\dot{\psi}$ in the negative mode, $\dot{\phi}$ does not change sign, and the windward meridian therefore rotates continuously in one direction. Since, as was shown above, the negative $\dot{\psi}$ mode is more stable, the windward meridian is more likely to be rotary, but either mode may persist, depending on the roll history.
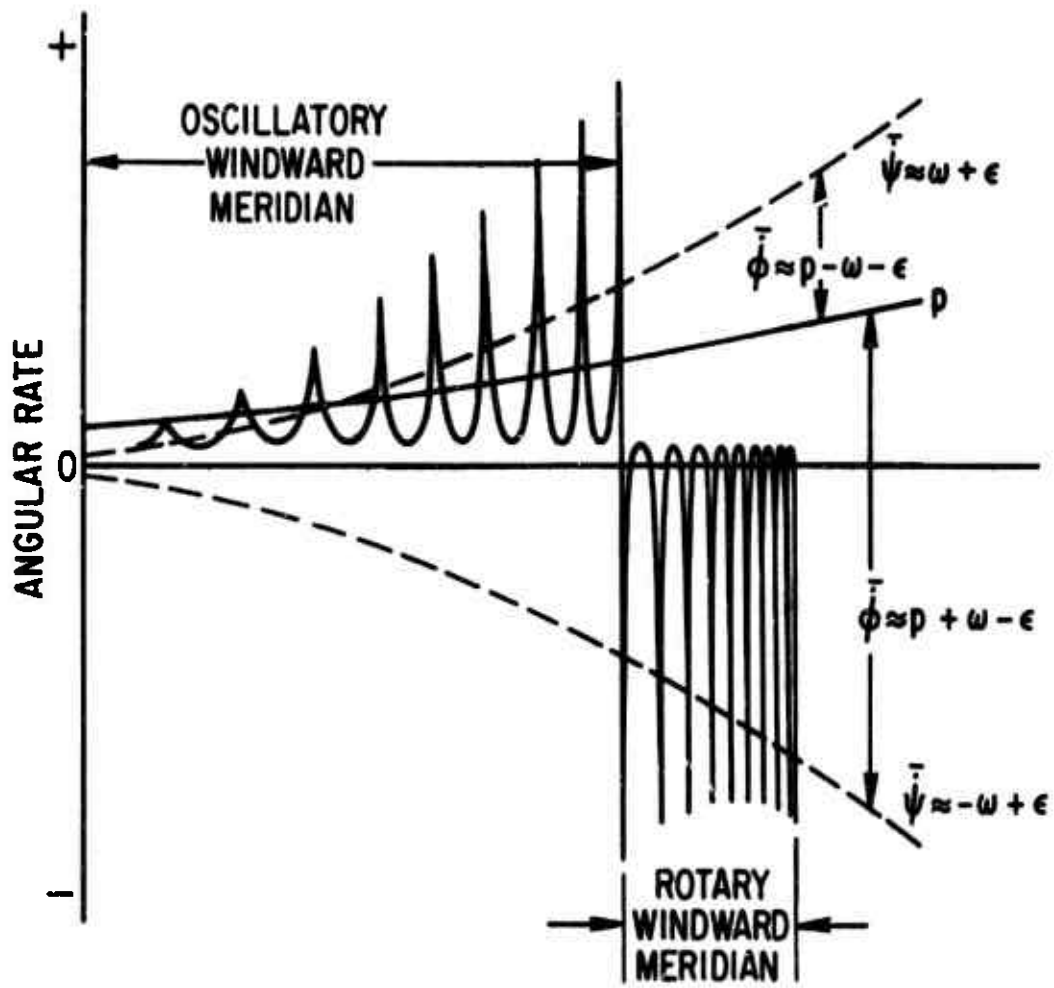
Figure 10. Windward Meridian Behavior

VI. COMPUTER SOLUTIONS

Figures 11 and 12 show computer solutions of the equations of motion, Eqs. (4), for the angle of attack and angular rates corresponding to the two limiting cases of exoatmospheric motion shown in Fig. 5. Also shown for comparison with the computer results are quasi-steady approximations for the angle-of-attack convergence, calculated from Eq. (15). Figure 11 corresponds to Fig. 5a, in which the rolling vehicle is at angle of attack with respect to the flight path, but has no precession. Figure 12 corresponds to the other limiting case, in which the vehicle is precessing initially about the average flight path in the positive direction.

Since the precession rate $\dot{\psi}$ is initially zero for the case of Fig. 11, and $\dot{\psi} = 0 < \mu p/2$, the vehicle will precess in the negative mode following reentry and will remain in the negative mode until the angle of attack approaches trim. This is verified from the computer result. Alternatively, for the case of Fig. 12, $\dot{\psi}$ is initially positive and greater than the reduced frequency $\mu p/2$. Therefore, $\dot{\psi}$ continues to precess in the positive mode and remains positive as long as the minimum value of the oscillation envelope reamins greater than $\mu p/2$. The reduced frequency is also plotted in Fig. 12 and remains less than the minimum value of $\dot{\psi}$ throughout the trajectory. Consequently, $\dot{\psi}$ remains in the positive mode, as verified by the computer result.

Figure 13 corresponds to a reentry in which the vehicle is coning initially about an axis inclined to the flight path. The precession rate $\dot{\psi}$ with respect to the flight path is positive initially and oscillates with an upper and lower bound. The lower bound is plotted against the reduced roll rate in Fig. 14 and is greater than $\mu p/2$ initially. However, the roll rate increases because of an applied roll torque, and the reduced roll rate approaches the minimum value of $\dot{\psi}$ after approximately 8 sec, which causes $\dot{\psi}$ to become unstable. Simultaneously, the lower bound of the angle-of-attack oscillation
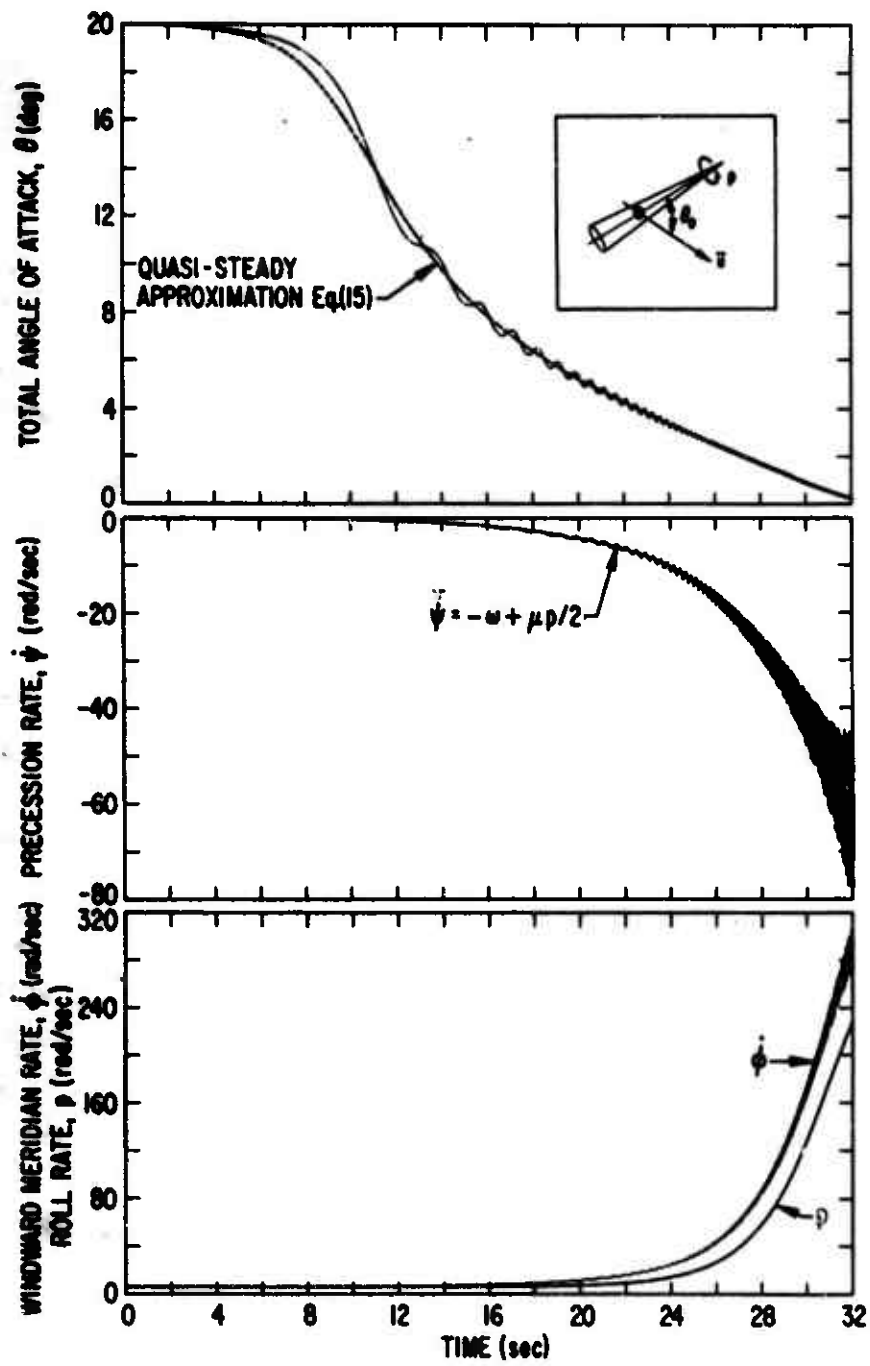
Figure 11. Motion History for Non-precessing Vehicle at Reentry
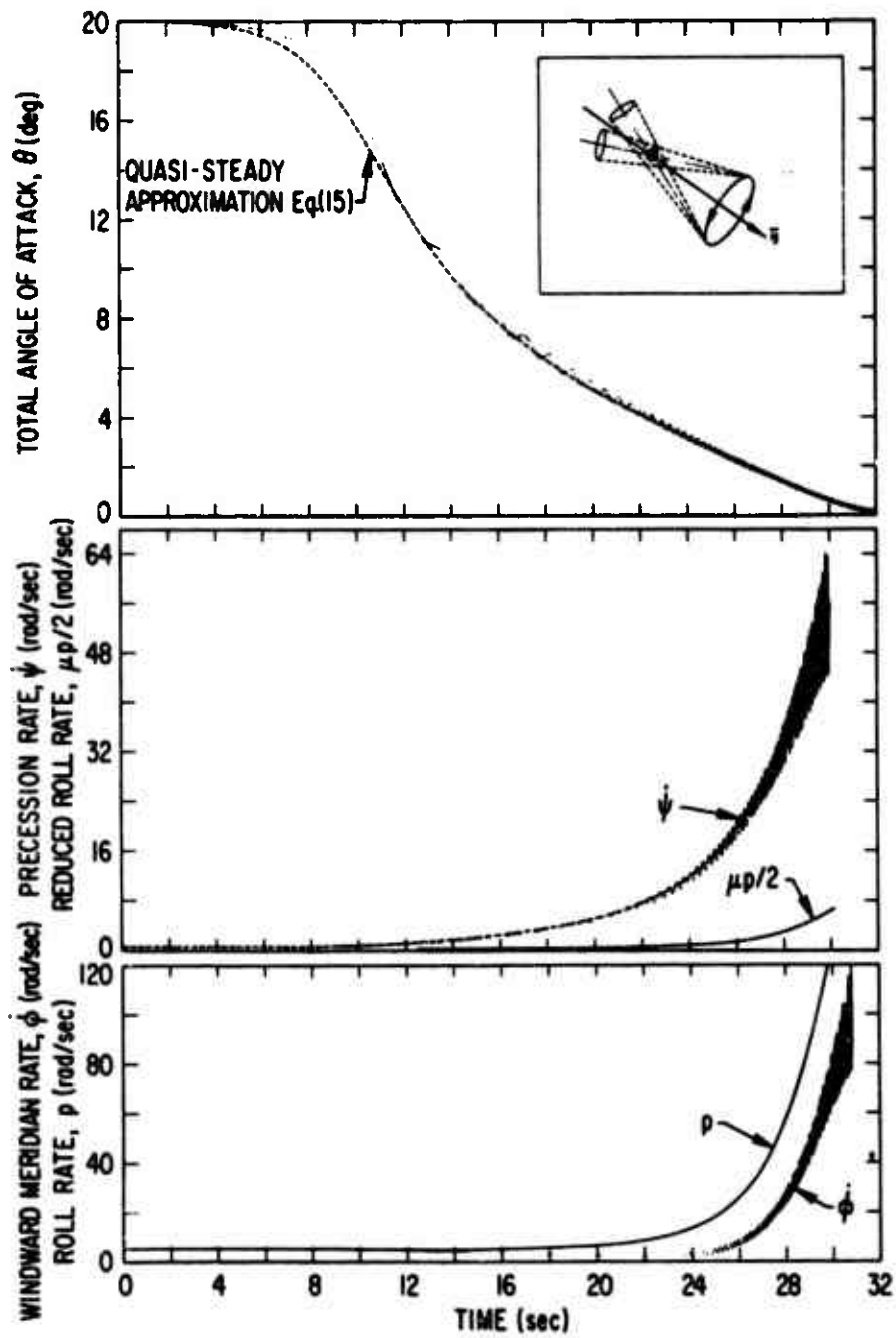
-36-

Figure 12. Motion History for Symmetric Precession
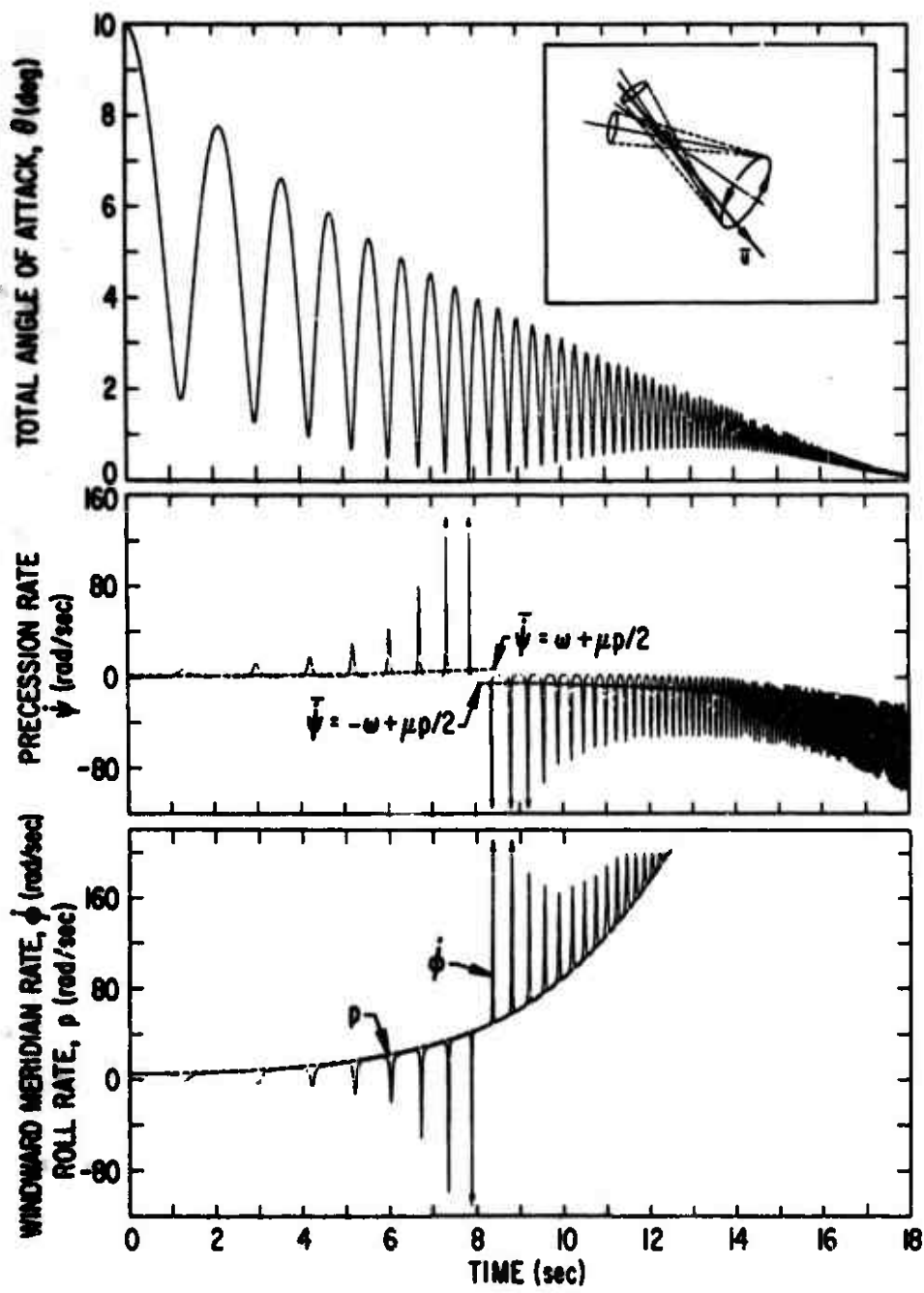About Flight Path at Reentry

Figure 13. Motion History for Unsymmetric Precession
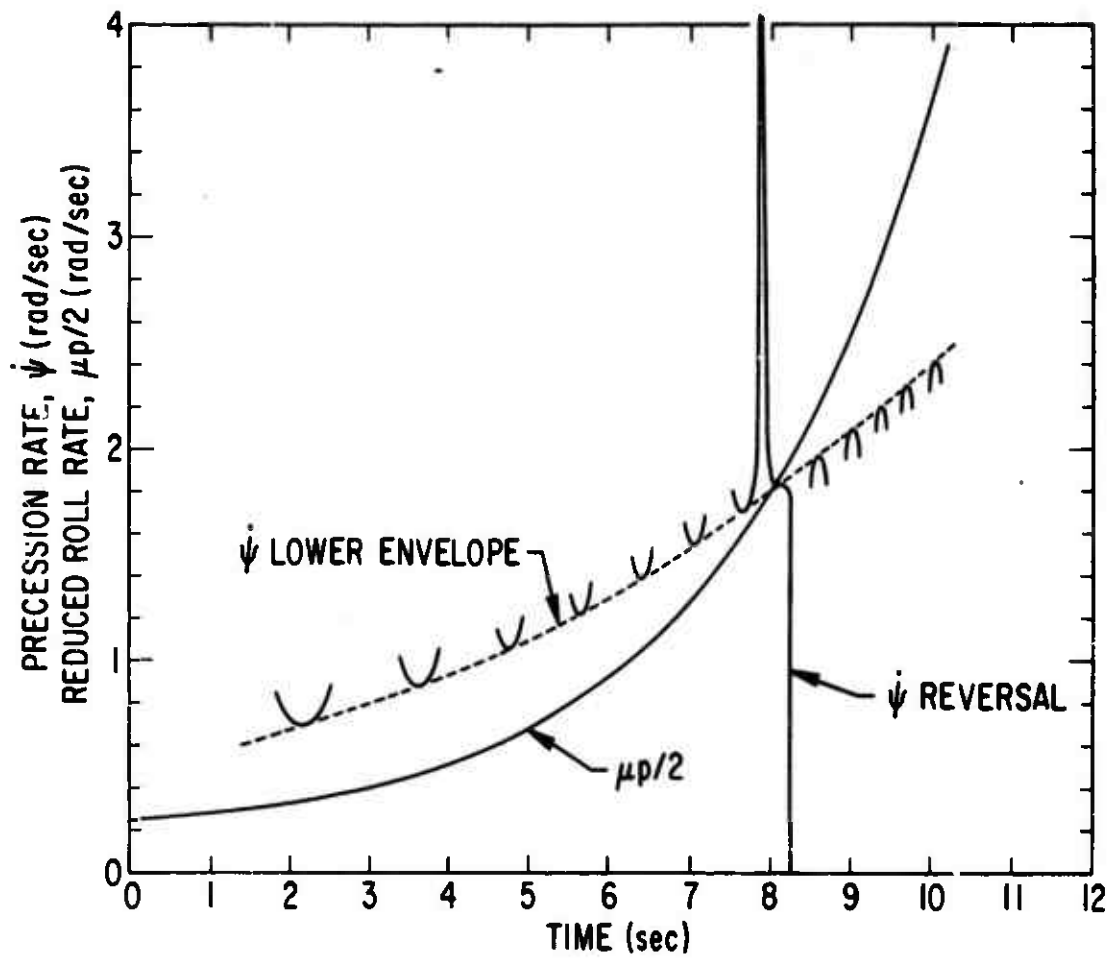About Flight Path at Reentry

Figure 14. Precession Instability

envelope approaches zero as the upper bound of $\dot{\psi}$ diverges, and $\dot{\psi}$ reverts to the more stable negative mode. The character of the motion also changes after the instability, as shown in Fig. 15, which is a polar plot of the angle of attack versus the precession angle ψ. Before the instability, the motion is characterized by "flower petal" loops containing the origin, whereas after the instability, the loops do not contain the origin (retrograde precession).
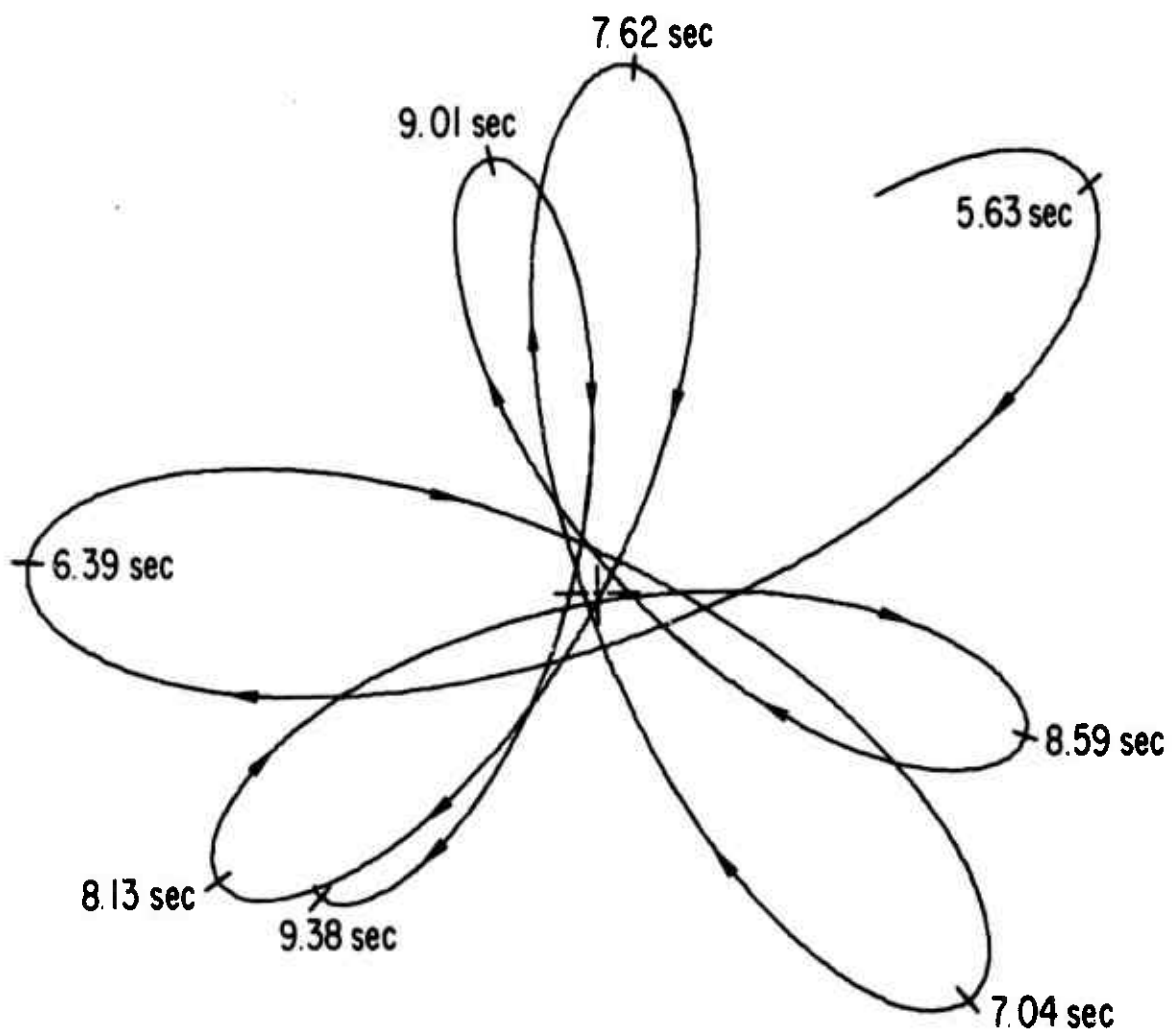
Figure 15. Polar Plot of Angle of Attack Before and
After Precession Instability

VII. SUMMARY AND CONCLUSIONS

A simple expression has been derived for the angle-of-attack convergence of a rolling reentry vehicle subject to roll acceleration and including pitch and yaw damping. The analytical result has been shown to compare favorably with computer solutions of the equations of motion. The effect of roll acceleration on the angle-of-attack convergence envelope is identical to the effect of pitch or yaw damping in the term $\dot{p}/p$, which either adds to or substracts from the damping coefficient, depending on the direction of the roll acceleration. The cumulative effects of damping and roll acceleration on the convergence envelope can be significant in certain cases. The angle-of-attack convergence also depends slightly on the mode of precession motion, which depends, in turn, on the initial reentry conditions.

It has been shown that a rolling reentry vehicle has two modes of precession motion, either of which can persist, depending on the initial reentry conditions and on the roll history. The positive mode is quasi-stable and will persist as long as the lower envelope of the precession rate oscillation ($\dot{\psi}$) is greater than the reduced roll rate parameter $\mu p/2$. If this parameter increases because of roll acceleration until it reaches the lower envelope of the $\dot{\psi}$ oscillation, a precession instability will occur, and the precession rate will change from the positive mode to the more stable negative mode. At the point of instability, the lower envelope of the angle-of-attack oscillation reaches zero. Following the instability, the angle of attack increases slightly, depending on the magnitude of the roll acceleration and on the pitch & yaw damping. The character of a polar plot of angle of attack vs precession angle also changes from "flower petal" loops containing the origin, before the instability, to loops that do not contain the origin, after the instability.

REFERENCES

1. T. B. Garber, "On the Rotational Motion of a Body Reentering the Atmosphere," J. Aerospace Sci. 26 (7), 443-449 (1959).

2. H. I. Leon, "Angle of Attack Convergence of a Spinning Missile Descending Through the Atmosphere," J. Aerospace Sci. 25 (8), 480-484 (1958).

3. M. Tobak and V. L. Peterson, Angle-of-Attack Convergence of Spinning Bodies Entering Planetary Atmospheres at Large Inclinations to the Flight Path, NASA TR R-210, Ames Research Center, Moffet Field, Calif. (October 1964).

4. C. L. Longmire, Reentry of Rotating Missiles, Research Note 213, Avco Everett Research Laboratory, Avco Corp., Everett, Mass. (December 1960).

5. F. A. Albini, Oscillation Envelope for a Spinning Reentry Vehicle, Report 21838, Hughes Aircraft Co., Space Systems Division, El Segundo, Calif. (27 February 1962).

6. W. T. Thomson, Introduction to Space Dynamics, John Wiley and Sons, Inc., New York (1961).

7. J. D. Nicolaides, On the Free Flight Motion of Missiles Having Slight Configurational Asymmetries, Report BRL-858, Ballistic Research Labs., Aberdeen Proving Ground, Md. (June 1953).

8. J. L. Synge and B. A. Griffith, Principles of Mechanics, 2nd ed., McGraw-Hill Book Co., Inc., New York (1949).

9. J. J. Stoker, Nonlinear Vibrations in Mechanical and Electrical Systems, Interscience Publishers, Inc., New York (1950).

10. P. M. DeRusso, et al., State Variables for Engineers, John Wiley and Sons, Inc., New York (1965).

DOCUMENT CONTROL DATA - R&D
(Security classification of title, body of abstract and indexing annotation must be entered when the overall report is classified)

1. ORIGINATING ACTIVITY *(Corporate author)*	2a. REPORT SECURITY CLASSIFICATION
The Aerospace Corporation, El Segundo, Calif.	Unclassified
	2b. GROUP

3. REPORT TITLE

ANGLE-OF-ATTACK CONVERGENCE AND WINDWARD-MERIDIAN
ROTATION RATE OF ROLLING REENTRY VEHICLES

4. DESCRIPTIVE NOTES *(Type of report and inclusive dates)*

5. AUTHOR(S) *(Last name, first name, initial)*

Platus, Daniel H.

6. REPORT DATE	7a. TOTAL NO. OF PAGES	7b. NO. OF REFS
69 JAN 08	44	10

8a. CONTRACT OR GRANT NO.	9a. ORIGINATOR'S REPORT NUMBER(S)
F04701-68-C-0200	
b. PROJECT NO.	TR-0200(4240-30)-3
c.	9b. OTHER REPORT NO(S) *(Any other numbers that may be assigned this report)*
d.	SAMSO-TR-69-53

10. AVAILABILITY/LIMITATION NOTICES

This document has been approved for public release and sale; its distribution is unlimited.

11. SUPPLEMENTARY NOTES	12. SPONSORING MILITARY ACTIVITY
	Space and Missile Systems Organization
	Air Force Systems Command
	United States Air Force

13. ABSTRACT

A simple expression is derived for the influence of roll acceleration on the angle-of-attack convergence of rolling reentry vehicles with pitch or yaw damping. Also included is an analysis of the windward-meridian rotation rate of the rolling vehicle, which is coupled through the gyroscopic equations of motion to the angle of attack and roll rate. It is found that two modes of motion exist for which the windward meridian is generally oscillatory in one mode and rotary in the other (i.e., the vehicle either oscillates about its roll axis relative to the wind or rotates continuously in one direction). The mode of motion depends on the initial reentry conditions, and it is shown that a roll-induced instability can occur whereby the motion changes from the oscillatory mode to the more stable rotary mode. The analytical approximations are compared with computer solutions of the complete equations of motion.

DD FORM 1473
(FACSIMILE)

14	KEY WORDS

Angle-of-attack convergence
Dynamic stability
Reentry vehicle
Reentry vehicle roll dynamics

Abstract (Continued)